Multistability and evolution of chimera states in a network of type II Morris–Lecar neurons with asymmetrical nonlocal inhibitory connections

O. Dogonasheva, Dmitry Kasatkin, Boris Gutkin, Denis Zakharov

Chaos
An Interdisciplinary Journal of Nonlinear Science

Multistability and evolution of chimera states in a network of type II Morris–Lecar neurons with asymmetrical nonlocal inhibitory connections

Cite as: Chaos **32**, 101101 (2022); https://doi.org/10.1063/5.0117845
Submitted: 02 August 2022 • Accepted: 12 September 2022 • Published Online: 07 October 2022

O. Dogonasheva, Dmitry Kasatkin, Boris Gutkin, et al.

Multistability and evolution of chimera states in a network of type II Morris–Lecar neurons with asymmetrical nonlocal inhibitory connections

Cite as: Chaos **32**, 101101 (2022); doi: 10.1063/5.0117845
Submitted: 2 August 2022 · Accepted: 12 September 2022 ·
Published Online: 7 October 2022

O. Dogonasheva,[1,2] Dmitry Kasatkin,[3] Boris Gutkin,[1] and Denis Zakharov[2,a)]

AFFILIATIONS

[1]Group of Neural Theory, École Normale Supérieure PSL University, Paris 75005, France
[2]Centre for Cognition and Decision Making, National Research University Higher School of Economics, Moscow 101000, Russia
[3]Department of Nonlinear Dynamics, Institute of Applied Physics RAS, Nizhny Novgorod 603155, Russia

[a)]**Author to whom correspondence should be addressed:** dgzakharov@hse.ru

ABSTRACT

Formation of synchronous activity patterns is an essential property of neuronal networks that has been of central interest to synchronization theory. Chimera states, where both synchronous and asynchronous activities of neurons co-exist in a single network, are particularly poignant examples of such patterns, whose dynamics and multistability may underlie brain function, such as cognitive tasks. However, dynamical mechanisms of coherent state formation in spiking neuronal networks as well as ways to control these states remain unclear. In this paper, we take a step in this direction by considering the evolution of chimera states in a network of class II excitable Morris–Lecar neurons with asymmetrical nonlocal inhibitory connections. Using the adaptive coherence measure, we are able to partition the network parameter space into regions of various collective behaviors (antiphase synchronous clusters, traveling waves, different types of chimera states as well as a spiking death regime) and have shown multistability between the various regimes. We track the evolution of the chimera states as a function of changed key network parameters and found transitions between various types of chimera states. We further find that the network can demonstrate long transients leading to quasi-persistence of activity patterns in the border regions hinting at near-criticality behaviors.

Over the past few decades, one of the most exciting and quickly developed areas of modern synchronization theory is the study of chimera states. Such chimera states are characterized by the coexistence of multiple synchronous and asynchronous domains despite that the network topology does not predict such structures. Moreover, these states are of interest for describing, for example, a partially synchronous activity in the brain neuronal networks and circuits. During cognitively effortful tasks, one can observe complex patterns of synchronous and non-synchronous brain activities that wax, wane, and reshape themselves, either rapidly or slowly, as the task demands. We may posit that dynamics of chimeras and their multistability may be key to how brain networks form activity patterns that allow implementation of such complex cognitive tasks (e.g., contextual memory states, multi-item working memory). In this work, we study the evolution of chimera states in a network of Morris–Lecar neurons whose excitability properties echo those of a major class of cortical interneurons and are arranged in a network with asymmetrical nonlocal inhibitory connections mimicking interneuronal networks in the cortex and hippocampus. Using a new measure of network coherence that we have previously introduced [the adaptive coherence measure (ACM)], we partition the network state space into regions with a variety of collective behaviors, antiphase synchronous clusters, traveling waves, different types of chimera states as well as spiking death regime, and uncover multistability between these various regimes. We followed how the various chimera states evolve from one to another with key network parameters and found that these switches can be either fast or that the network can demonstrate long transients, leading to quasi-persistence of activity patterns in the border regions hinting at near-criticality behaviors. Hence, our work shows that spiking networks with even relatively simple connection topologies are capable of complex dynamics, as they may underlie cognitively relevant brain activities.

I. INTRODUCTION

Multistability plays a key role in the control of activity in neuronal networks. Multi-stable states, or multiple attractors, may also appear during the performance of cognitive tasks and processes (such as multi-item decision-making tasks), which in turn endow multistability with a functional significance. To flexibly switch between multiple cognitive tasks successfully, network activity patterns need to be flexibly restructured, and it is here that network multistability can be a potential mechanism. Interestingly, switching between multiple activity patterns may need to be rapid (to change between tasks) or with long-lasting quasi-stable dynamics, e.g., to implement working memory functions.[1–3] Multistable dynamic patterns may be heterogeneous in their structure (depending on the cognitive task) and are unlikely to be fully globally synchronous. One can argue that such complex task-related network patterns may consist of multiple synchronous (or coherent) neuronal populations that are directly involved in computations necessary for the task at hand as well as populations that are not involved in the task and that may be asynchronous. In terms of nonlinear dynamics, such mixed states are known as chimera states.[4] Over the past few years, the study of chimera states has been one of the main directions in synchronization theory (see, for example, overview[5] and papers cited within). Arguably, one of the central challenges for synchronization theory and network studies in computational neuroscience is to identify the mechanisms that are responsible for the formation of such dynamic activity patterns.

Initially, chimera states were found in homogeneous networks with a symmetrical connection structure.[4] However, such a symmetric network topology is quite unlikely to be observed in biological neuronal networks. As a rule, neurons follow Dale's law and interact mainly through (either excitatory or inhibitory) chemical synapses. This means that such couplings are unidirectional, where the electrochemical synaptic signals are transmitted from the presynaptic neuron to the postsynaptic ones (see, for example, Ref. 6). Another point is that connection topology, in general, is not symmetric, as previously discussed in Ref. 7. Moreover, experimental data show that unidirectional connections are widespread in biological neural networks and play an essential role in the computational capabilities of the brain (see, for example, Ref. 8). Thus, it is of importance to generalize chimera states to neuronal networks with more realistic brain-network and neural circuit connectivity properties.

There have been a number of studies devoted to studying chimera states in neuronal networks, and most of them consider nonlocal ring typologies. For example, one of the earliest seminal works in this field is devoted to a ring consisting of Hodgkin–Huxley neurons,[9] where the strength of the connection decreases with the distance between the neurons. For the cases of both excitatory and inhibitory synaptic couplings, they found states resembling chimera states. Later, static chimera and multichimera chimera states were discovered for a ring network of the FitzHugh–Nagumo neurons[10] as well as for an excitatory coupled ring of Morris–Lecar neurons with class I excitability.[11] Chimera states were also discovered in rings of bursting neurons[12,13] as well as traveling chimera states,[12,14] where the asynchronous domains move along the ring. Once again, these studies considered symmetric coupling patterns.

Furthermore, from a biological point of view, we could note that the two major classes of neurons in the cortex differ in their spike-generating dynamical properties (or excitability classes). Typically, cortical pyramidal neurons appear to be of class I excitability and are excitatory, whereas interneurons (at least one large class of them—the fast spiking interneurons) are of class II excitability[15] and are inhibitory. Thus, it is of interest to understand how not only the connectivity structure, but also the intrinsic excitability dynamics define and sculpt the collective dynamics of networks of neurons. For example, one prominent study[11] considered a ring of Morris–Lecar neuron class I excitability (pyramidal cells) with nonlocal excitatory connectivity where static chimera states were observed. In Ref. 10, a ring of the FitzHugh–Nagumo elements, which are typically class II excitability, of static multichimera were discovered. However, the authors in both of these studies used the nonsynaptic (biologically unrealistic) connections, and thus, the question of collective dynamics of a ring of interneurons with biologically plausible connections is still open. In this paper, we approach this question by considering a ring of Morris–Lecar class II excitable neurons with inhibitory connections. Moreover, we choose a uni-directional nonlocal connectivity topology that has been earlier proposed as a model for encoding sequences and sequential information flow (see, for example, Ref. 16).

II. THE MODEL

We consider a ring of Morris–Lecar neurons[17] coupled nonlocally with inhibitory chemical synapses,

$$\begin{cases} C\dot{V}_i = I_{app} - g_{Ca} m_i^{inf}(V_i - E_{Ca}) \\ \qquad\qquad - g_K w_i (V_i - E_K) - g_L (V_i - E_L) + I_i^{syn}, \\ \dot{w}_i = \phi (w_i^{inf} - w_i) \cosh \dfrac{V_i - V_3}{2V_4}, \\ w_i^{inf} = 0.5\left(1 + \tanh \dfrac{V_i - V_3}{V_4}\right), \\ m_i^{inf} = 0.5\left(1 + \tanh \dfrac{V_i - V_1}{V_2}\right), \end{cases} \tag{1}$$

where $i \in 1, \ldots, N$, where N is the total neuron number; C is a membrane capacity; V_i is a membrane potential of the ith neuron; w_i and m_i are gating variables of K^+ and Ca^{2+} channels; E_K, E_{Ca}, and E_L are the reversible potentials for potassium, calcium, and leak channels, respectively; g_K, g_{Ca}, and g_L are their conductances; and I_{app} is an applied current. We set the neuronal parameters in a way to provide neurons to be class II excitability.

Inhibitory (γ-aminobutyric acid-A, $GABA_A$) synaptic current supplied to the ith neuron is described by the first order kinetics,[6]

$$\begin{cases} I_i^{syn} = \dfrac{g_{syn}}{N} \displaystyle\sum_{j=i+1}^{i+R} x_j (V_R - V_i), \\ \dot{x}_j = \alpha \dfrac{1}{1 + \exp\left(-\frac{V_j - V_{syn}}{K_p}\right)} (1 - x_j) - \beta x_j. \end{cases} \tag{2}$$

TABLE I. The fixed neuronal network parameters.

$g_K = 8\,\mathrm{mS/cm^2}$	$E_K = -80\,\mathrm{mV}$	$V_1 = -1.2\,\mathrm{mV}$	$\alpha = 1.1$
$g_{Ca} = 4.4\,\mathrm{mS/cm^2}$	$E_{Ca} = 120\,\mathrm{mV}$	$V_2 = 18\,\mathrm{mV}$	$\beta = 0.19$
$g_L = 2\,\mathrm{mS/cm^2}$	$E_L = -60\,\mathrm{mV}$	$V_3 = 2\,\mathrm{mV}$	$N = 500$
$\phi = 1/25$	$C = 20\,\mu\mathrm{F/cm^2}$	$V_4 = 30\,\mathrm{mV}$	$K_p = 5$
$V_{syn} = 2\,\mathrm{mV}$	$V_R = -60\,\mathrm{mV}$		

Here, g_{syn} is the synaptic strength, V_R is the reversal potential, V_{syn} is the threshold, K_p is the synaptic activation, x_i is the fraction of open receptors on the postsynaptic membrane of the ith neuron, and R is the number of connections directed only in one way (clockwise or counterclockwise) along the ring. As usual, we define the connectivity parameter $r = \frac{R}{N}$ that describes the connection density of the network.

To study the network states, we fix all parameters (Table I) except the control parameters: external current I_{app}, synaptic strength g_{syn}, and connectivity parameter r.

III. METHODS

To identify the dynamical regimes of the network, we use the adaptive coherence measure (ACM).[18] The criterion is based on the χ^2-parameter[19] and involves the optimization problem,

$$R^2 = \max_{\Delta\mathbf{t}=(\Delta t_1, \Delta t_2, \ldots, \Delta t_N)} \chi^2\left(\{V_i(t-\Delta t_i)\}_{i=1}^N\right), \tag{3}$$

where $\Delta\mathbf{t} = (\Delta t_1, \Delta t_2, \ldots, \Delta t_N)$ is a time delay vector that contains L unique time lags and χ^2 is defined as follows:

$$\chi^2 = \frac{\sigma_V^2}{\frac{1}{N}\sum_{i=1}^N \sigma_{V_i}^2}, \tag{4}$$

where σ_V^2 is the variance of the average membrane potential of the network $V(t) = \frac{1}{N}\sum_{i=1}^N V_i(t)$ and $\sigma_{V_i}^2$ is variance of the membrane potential of the ith neuron.

Using both criteria (the number of unique time lags L and the value of R^2), one can easily identify a dynamical regime.[18] If R^2 is close to zero, an asynchronous state is observed. For a chimera state, its value ranges from zero to one: $0 < R^2 < 1$. In the other cases of global synchronization, states consisting of only synchronous clusters and traveling waves, R^2 is close to one, and to classify the states, we need to use the number of unique delays L. For traveling waves, L is equal to N/k (k is the number of waves in the ring); for a clustered state, it is between 1 and N, and for global synchronization, it is equal to 1. To find the speed of traveling chimera states, we use the method introduced in Refs. 18 and 20.

For numerical integration, the Euler method with a fixed step (100 μs) was used. The simulation time of Eqs. (1) and (2) was 30 s. To set this integration length, we first looked at longer simulations and found that 30 s is enough to have robust results. Even 2 s is more than enough to reliably identify the coherent states of the network (for more information, see the supplementary material). In addition, we note that 30 s allows one to integrate out any transients and many orders of magnitude longer than any intrinsic time scale in the network (e.g., membrane time constants, current kinetic constants, synaptic time constants).

IV. RESULTS

We find that the network (1) and (2) demonstrates multiple dynamical activity regimes: traveling waves, states with the two antiphase clusters, chimera states, and spiking death states. The corresponding maps of dynamical regimes for the parameter plane (r, g_{syn}) for $I_{app} = 95\,\mu\mathrm{A/cm^2}$ are presented in Fig. 1. The maps for the plane (I_{app}, g_{syn}) for $r = 0.4$ and $r = 0.89$ are available in Fig. S1 of the supplementary material. The main dynamical regimes were discovered by searching in the space of initial conditions and parameters. Thereafter, each region in these diagrams was plotted by a natural continuation algorithm[21] when the simulations started from the initial conditions obtained for the previous control parameter value and continued under a small parameter step.

As we see in Fig. 1, there are numerous intersections between the regions corresponding to the different states. In other words, the network typically demonstrates multistability. As in Ref. 22, at each set of parameters, depending on initial conditions, the network shows various collective dynamics. We can note that in the (r, g_{syn}) plane, there are several regions that are associated with chimera states: "Ch1," "Ch2," and "Ch3" (Fig. 1). Let us focus on the largest and most interesting region Ch1, and other regions are discussed in the supplementary material. This region contains an area, which has no intersection with the other regions and where we find only a static multichimera state. Figure 2 shows an example of such a state (corresponding to the parameter set of point A in Fig. 1: $I_{app} = 95\,\mu\mathrm{A/cm^2}$, $r = 0.89$, and $g_{syn} = 4.5\,\mathrm{mS/cm^2}$).

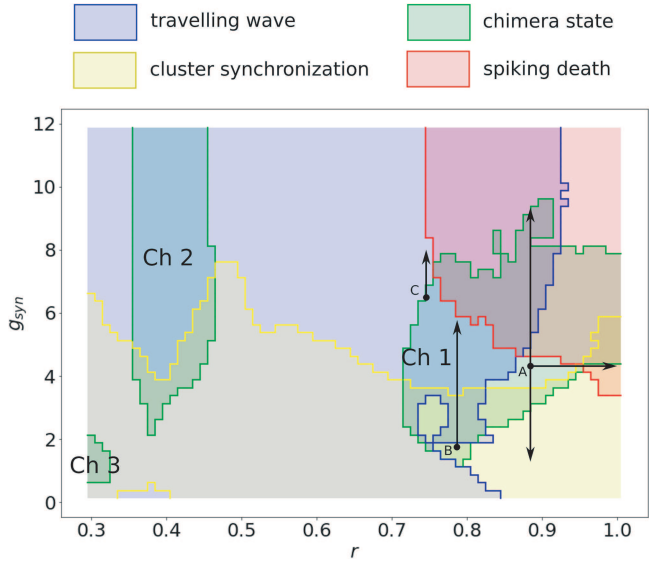

FIG. 1. Maps of the coherent states of the network (1) and (2): the parameter plane (r, g_{syn}) for fixed applied current $I_{app} = 95\,\mu\mathrm{A/cm^2}$. Regimes: traveling wave (blue), cluster synchronization (yellow), chimera state (green), and spiking death (red). Due to multistability, the regions intersect and their colors mix: for example, the gray color in the lower left corner is the intersection of the regions of traveling waves (blue) and cluster synchronization (yellow). The borders of the regions keep their own colors.

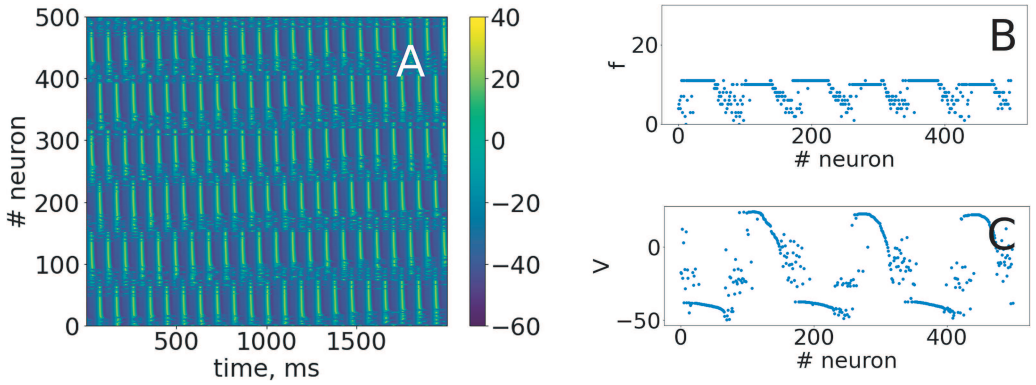

FIG. 2. A multichimera state: the raster plot (a), the frequency distribution (b), and the snapshot (c): $I_{app} = 95\ \mu A/cm^2$, $g_{syn} = 4.5\ mS/cm^2$, and $r = 0.89$.

A. Evolution of chimera states

Let us consider the evolution of this chimera state associated with point A in Fig. 1 when varying the control parameters g_{syn} and r.

For increasing synaptic strength g_{syn} and a fixed value $r = 0.89$ (moving up from point A in Fig. 1), we see successive transitions to a breathing chimera state [Fig. 3(a)], a traveling breathing chimera state [Fig. 3(b)], and, finally, to traveling waves [Fig. 3(d)]. Due to the abrupt change R^2 and L at the moment of transition to the traveling wave regime (see Fig. S14 and additional information in the supplementary material) and analysis of Fig. 1, we can conclude that the last transition happens through the disappearance of the traveling breathing chimera state and evolution of the network to the already existing regime of traveling waves.

When, on the other hand, we decrease the synaptic strength g_{syn} for the fixed value $r = 0.89$ (moving down from point A in Fig. 1), the incoherent domains of the multichimera state become smaller [Fig. 4(b)] and with further decreases of g_{syn} disappear completely. The network, in this case, evolves to a state with two antiphase clusters [Fig. 4(c)].

Moving from point A to the right by increasing the connectivity parameter r for the fixed synaptic strength ($g_{syn} = 5\ mS/cm^2$), the network also demonstrates a transition to a state with two antiphase clusters. The difference from the previous case is that along with the typical two cluster spiking state, there exists a state with two antiphase clusters for which neurons of one of the clusters show subthreshold voltage oscillations and never generate spikes. Note that despite the fact that mathematically, these two states are almost similar, and from a biological point of view, the difference between them is significant. Since spike generation is a critically important factor in the transmission, processing, and storage of information, the lack of spike generation in one of the clusters actually removes these neurons from information processing and also reduces the "population" frequency of the network by two times that can be observed experimentally.

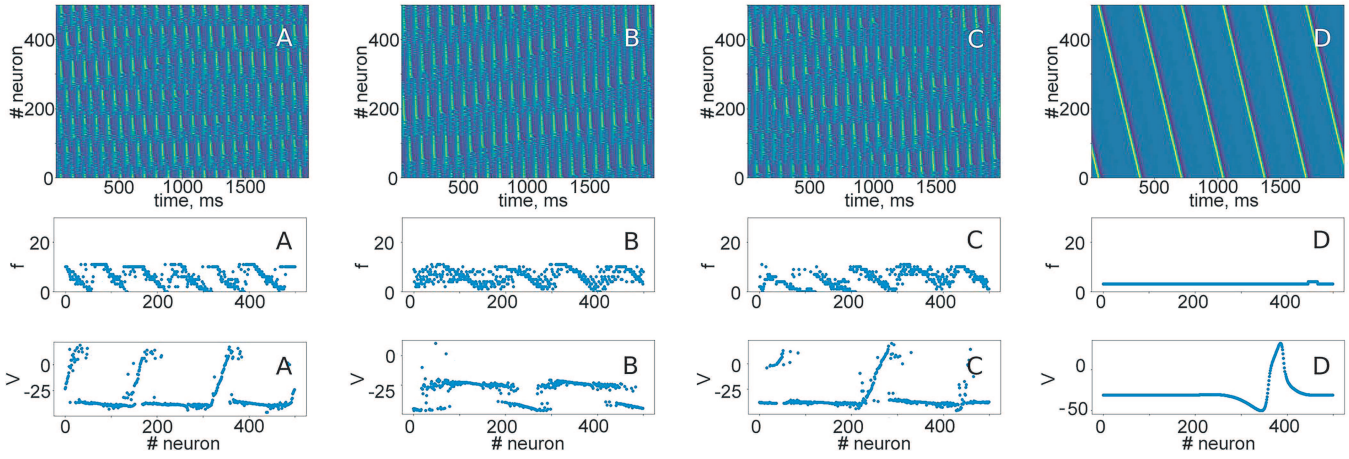

FIG. 3. Transition from a multichimera state to a breathing chimera state and further to traveling waves (moving down from point A in Fig. 1: $I_{app} = 95\ \mu A/cm^2$ and $r = 0.89$). The synaptic strength is $g_{syn} = 6.4\ mS/cm^2$ (a), $g_{syn} = 7.1\ mS/cm^2$ (b), $g_{syn} = 7.7\ mS/cm^2$ (c), and $g_{syn} = 7.9\ mS/cm^2$ (d).

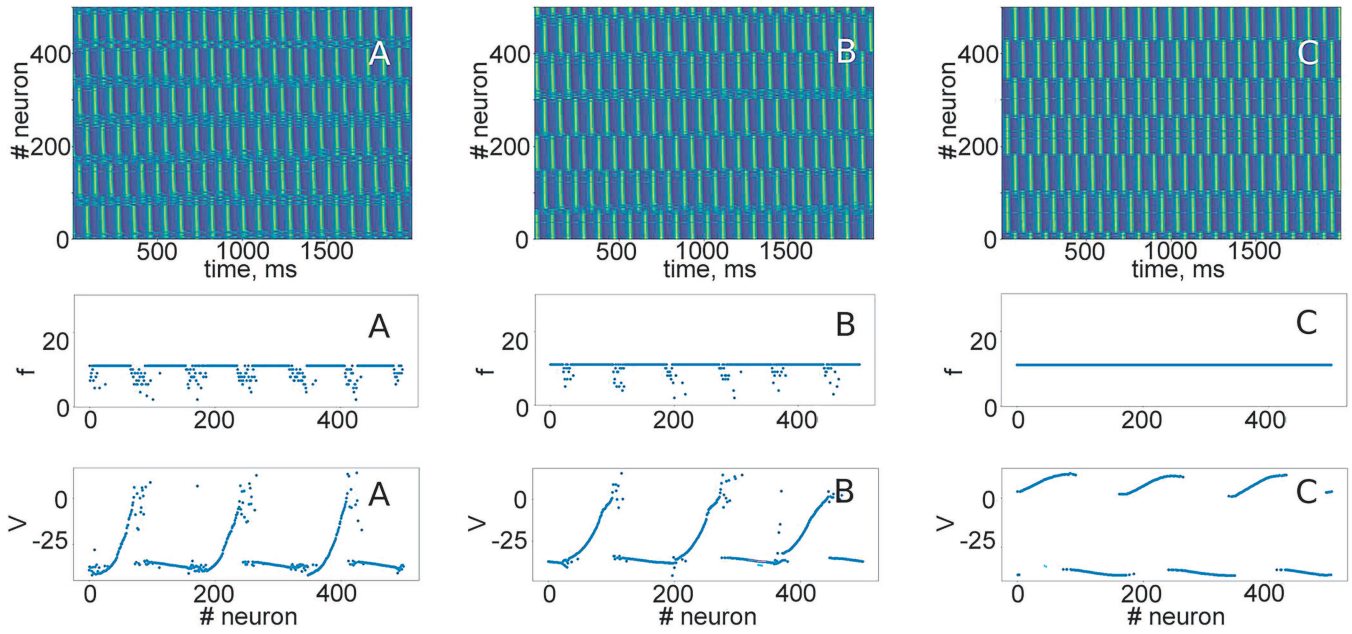

FIG. 4. Transition from a multichimera state to a synchronous regime with two antiphase clusters (moving down from point A in Fig. 1: $I_{app} = 95\,\mu\text{A/cm}^2$ and $r = 0.89$). The synaptic strength is $g_{syn} = 3.5\,\text{mS/cm}^2$ (a), $g_{syn} = 3\,\text{mS/cm}^2$ (b), and $g_{syn} = 2.5\,\text{mS/cm}^2$ (c).

In the left part of region *Ch*1, we observe a traveling multichimera state like at point B in Fig. 1 ($I_{app} = 95\,\mu\text{A/cm}^2$, $r = 0.79$ and $g_{syn} = 2\,\text{mS/cm}^2$). The raster plot, the frequency distribution, and the frequency diagram are presented in Fig. 5(a). With the growth of synaptic strength g_{syn}, the chimera speed increases, and in the frequency diagram [Figs. 5(b) and 5(c)], the "frequency oscillating tails" appear. These tails contain neurons generating spikes with various frequencies, and for sufficiently large synaptic strength, there are some neurons that stop generating spikes during finite time intervals. The number of neurons showing subthreshold oscillations becomes larger with increasing synaptic strength. We call such states complex multichimera states. The tails of complex multichimera states can consist almost entirely of subthreshold domains, such as in Fig. 6(a) (point C in Fig. 1; $I_{app} = 95\,\mu\text{A/cm}^2$, $r = 0.76$, and $g_{syn} = 6.5\,\text{mS/cm}^2$). With increasing synaptic strength, the subthreshold domains become smaller, and for large enough g_{syn}, there occurs a transition to traveling waves [Figs. 6(b) and 6(c)].

B. Slow transients

As we showed above, in most parameter regions, the network demonstrates multistability. This means that for the same parameter set, the network can exhibit various states depending on the initial conditions. This, in turn, allows control of the network regimes by altering external forcing or changing the initial conditions. When we looked into the time scales of transitions from one state to another, we found along with rapid switching that the network can demonstrate very long transient processes. Therefore, even if the initial conditions have changed, the transition from one dynamic regime to another one can take a long time, and this looks like a metastable state. For instance, if we move up from point A in Fig. 1 ($I_{app} = 95\,\mu\text{A/cm}^2$, $r = 0.89$, and g_{syn} grows), the network shows a transition from the static chimera state (Fig. 2) to the traveling chimera and further to traveling waves (Fig. 3). In particular, for $g_{syn} = 8.9\,\text{mS/cm}^2$, the network is able to demonstrate the traveling waves. However, if we start from the initial conditions corresponding to the already non-existent static breathing chimera state, the network keeps such activity for more than 6 s, and only after that state, traveling waves start to form (Fig. 7). For the cellular processes in the brain, 6 s is an extremely long time, orders of magnitude longer than any of the cellular time constants; hence, we see an emergence of ultra-slow-time scale dynamic behaviors. Such slow transients can also be observed for a transition between different states and, in particular, between chimera states. For example, a static multichimera may be suddenly replaced by a traveling multichimera after approximately 6 s (Fig. 8). Possible dynamical mechanisms of such transients are still unclear and require further research.

C. Influence of the applied current

Neuronal excitability, which is controlled by the parameter I_{app} in the network [Eqs. (1) and (2)], also plays a key role in collective activity of the network (see Fig. S1 in the supplementary material). For small values of the parameter, we observe a spiking death regime when only a small number of neurons in the network are active (see the supplementary material). With the growth of I_{app}, progressively more neurons become active, forming two antiphase clusters.

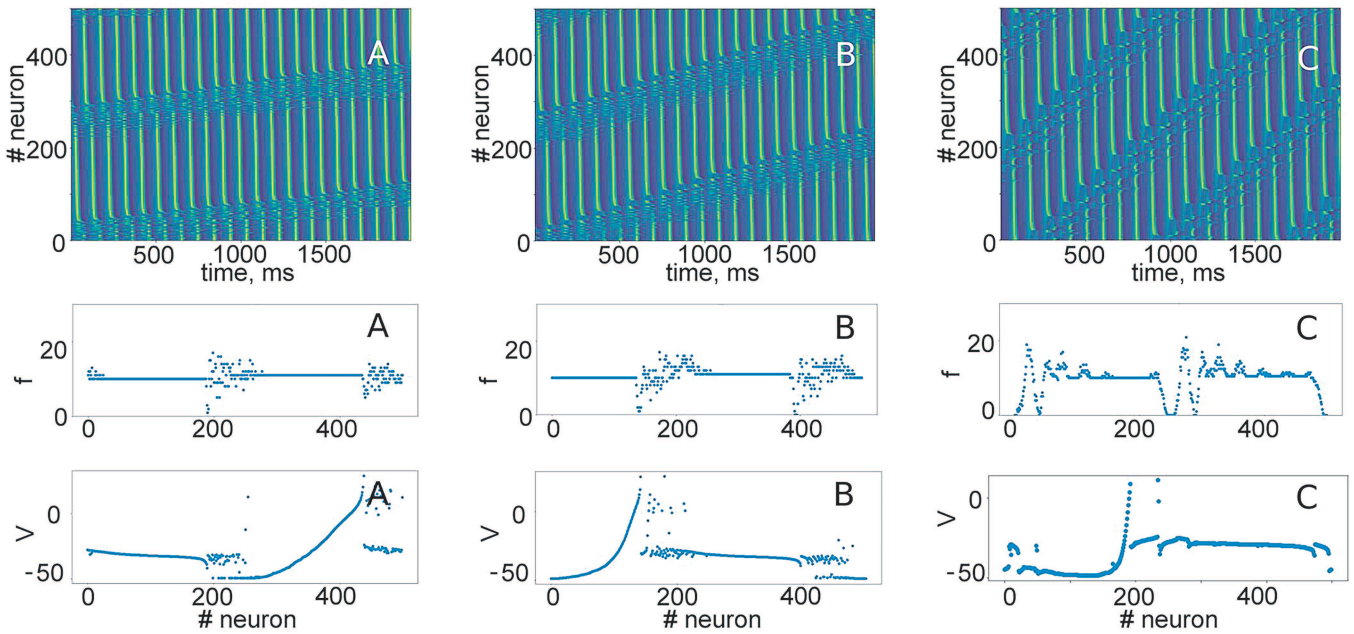

FIG. 5. Transition from a multichimera state to a complex multichimera state (moving up from point B in Fig. 1: $I_{app} = 95\,\mu\mathrm{A/cm^2}$ and $r = 0.79$). The synaptic strength is $g_{syn} = 2\,\mathrm{mS/cm^2}$ (a), $g_{syn} = 3.5\,\mathrm{mS/cm^2}$ (b), and $g_{syn} = 5.5\,\mathrm{mS/cm^2}$ (c).

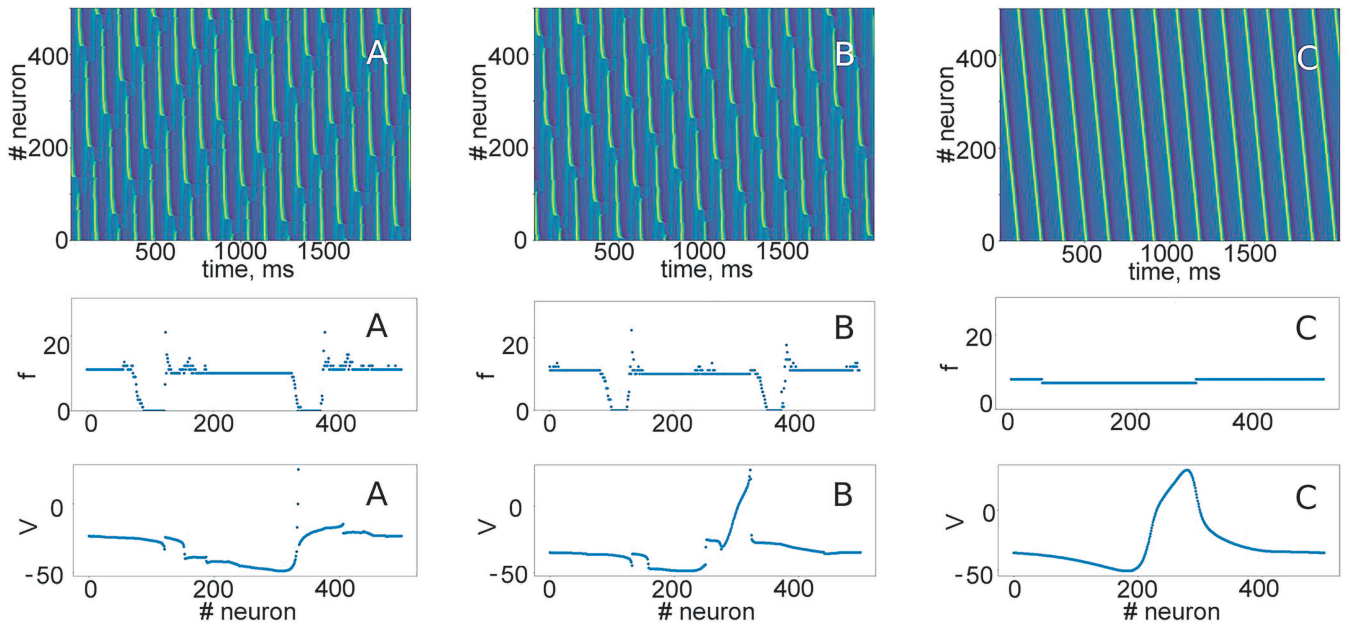

FIG. 6. Transition from a complex multichimera state containing large subthreshold domains to traveling waves (moving up from point C in Fig. 1: $I_{app} = 95\,\mu\mathrm{A/cm^2}$ and $r = 0.76$). The synaptic strength is $g_{syn} = 6.5\,\mathrm{mS/cm^2}$ (a), $g_{syn} = 7.5\,\mathrm{mS/cm^2}$ (b), and right: $g_{syn} = 8\,\mathrm{mS/cm^2}$ (c).

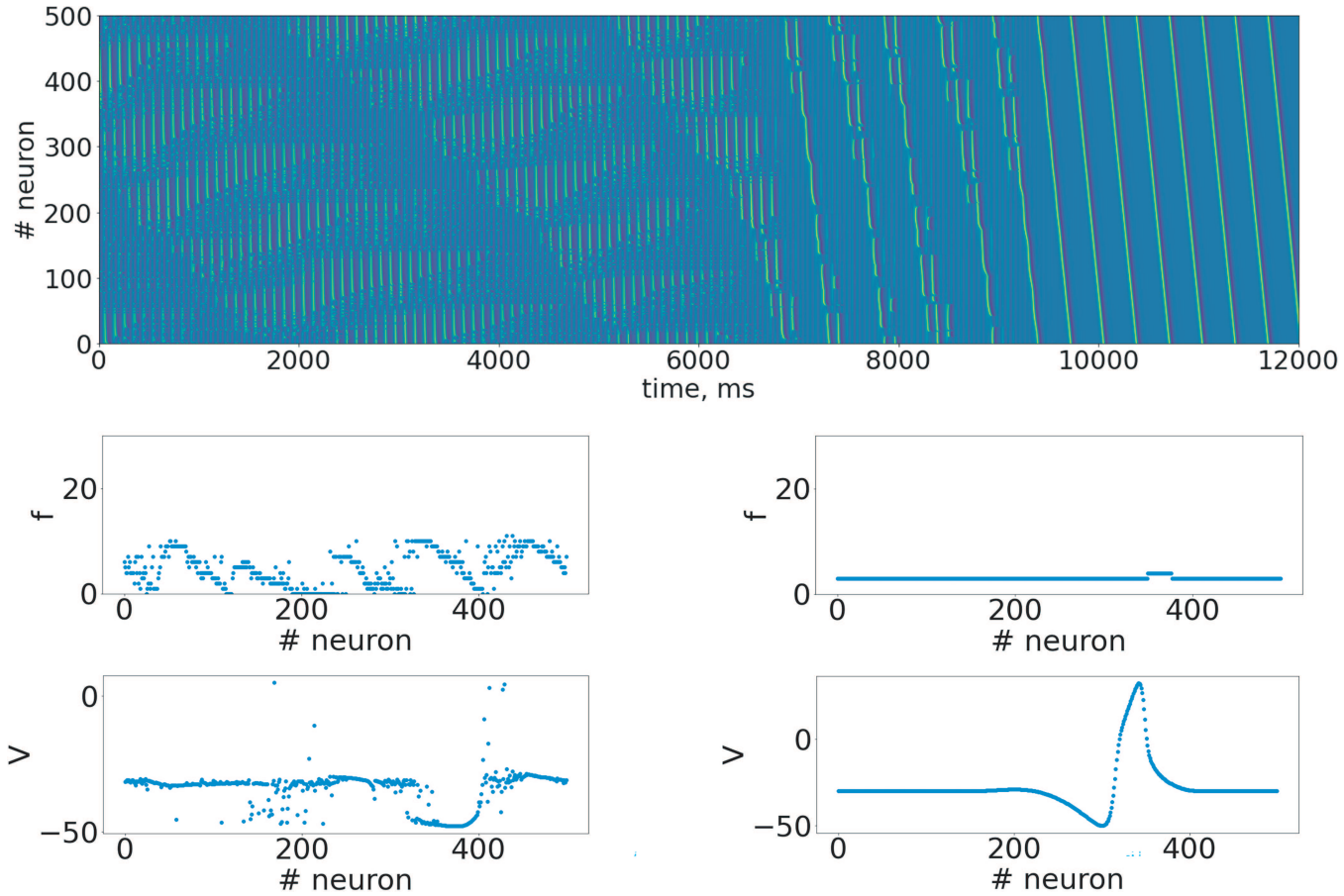

FIG. 7. Transient process from a breathing chimera to a traveling wave. Below, there are frequency diagrams and snapshots for (from left to right) $t = 4000$ and 11 000 ms, respectively. Parameters: $I_{app} = 95\ \mu\text{A/cm}^2$, $r = 0.89$, and $g_{syn} = 8.25\ \text{mS/cm}^2$.

For still higher values of the applied current, traveling waves become the most probable regime. Interestingly, chimera states coexist over a wide range of I_{app} with the other coherent states (clusters and/or traveling waves). Additional information about the impact of neuronal excitability on the activity pattern formation is given in the supplementary material.

V. DISCUSSION

In this paper, we made a step to connection asymmetry and considered a network of identical (excitability class II) Morris–Lecar neurons with nonlocal directed, yet homogeneous, inhibitory connections. We emphasize that the article is devoted not only to the study of the mechanism of chimeras, but also to the stability and features of chimera-like states in conditions of an imperfection of topology. We showed that even in the case of one-way connections, the chimera states still exist. In our network, all neurons are identical, all of them are interacting with other neurons (the network is not modular), and each neuron receives the same impact from the network in the sense that all neurons are connected with the same number of other neurons (all neurons have identical connectivity patterns). From this point of view, in spite of network asymmetry, there is an "interaction" symmetry, the network is homogeneous, and we can use the term "chimera state" when we observe that the network breaks up into synchronous and asynchronous domains.

To identify coherent states of the network (global synchronization, states with two asynchronous clusters, traveling waves, and chimera states), we used the ACM approach.[18] It was found that ACM performs very well. The advantages of ACM are that it does not have internal parameters, is able to distinguish all basic coherent states, and is thus applicable for continuous analysis and plotting 2D maps. Using this approach and the natural continuation algorithm, we partitioned the parameter space into regions of various network states and showed that multistability occurs for most sets of parameters (technical aspects of using the ACM approach are available in the supplementary material). Such multistability should allow control of the network state by external stimulation or initial condition changes. At the same time, we have shown that certain transitions between the network states can initiate the long transient processes

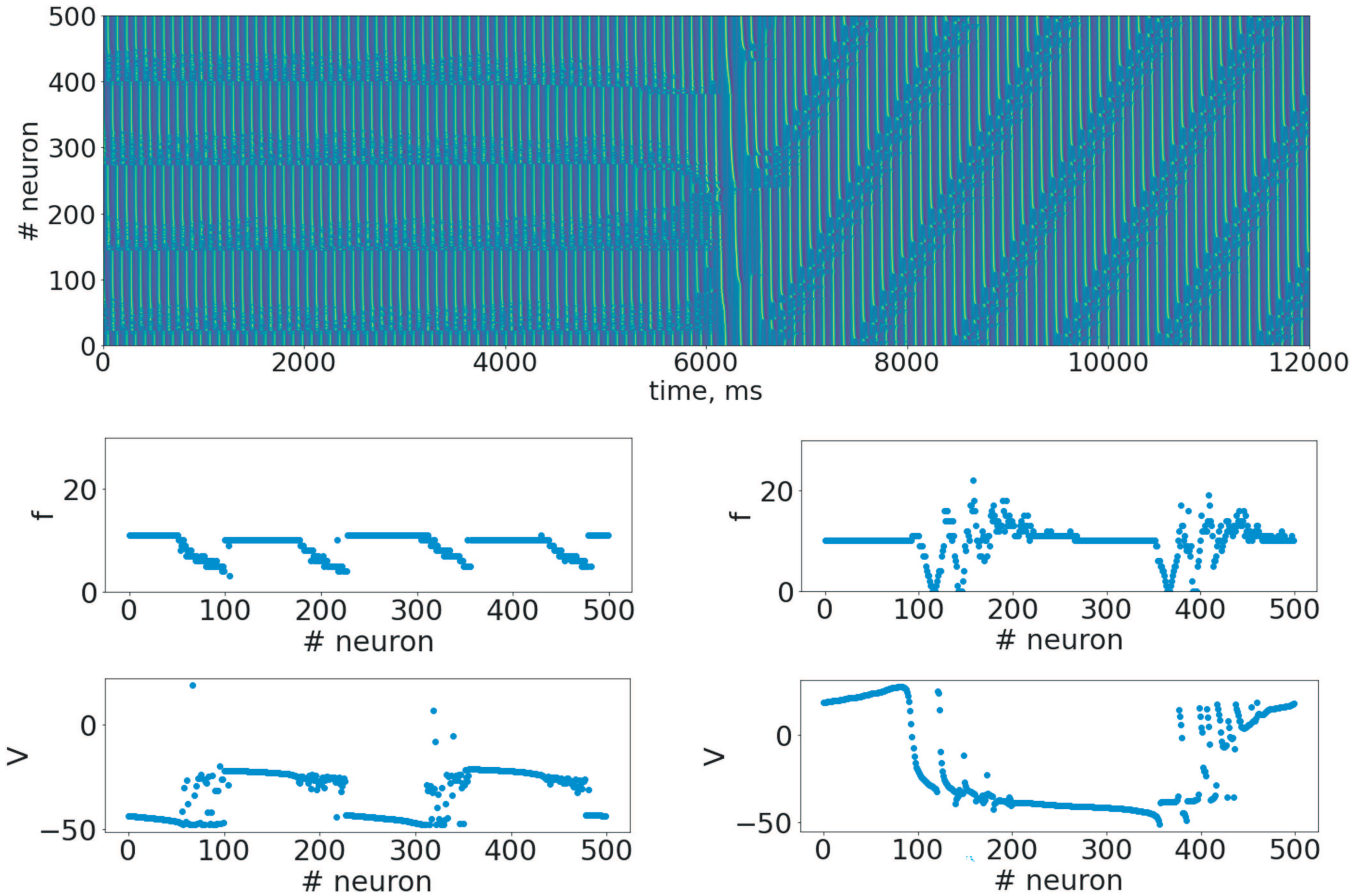

FIG. 8. Transient process from a static multichimera to a traveling multichimera. Below, there are frequency diagrams and snapshots for (from left to right) $t = 1000$ and 10 000 ms, respectively. Parameters: $I_{app} = 95\ \mu\text{A/cm}^2$, $r = 0.77$, and $g_{syn} = 4.5\ \text{mS/cm}^2$.

that can last far beyond any intrinsic time scales of the constituent neurons or their connections (more than several seconds).

Such long transients make it possible to consider the metastability of chimera states as an important aspect not only of attractor but also of transient (metastable) neuronal dynamics. For example, heteroclinic sequential dynamics have been suggested before and are based on robust heteroclinic cycles (or stable heteroclinic channels) implementing winnerless competition (see, for example, the review[23]). In our case, we have no sequential dynamics and trajectory without an external input after enough long interval approaches to a stable network state. In other words, we have shown that our network can have long transients whose duration (several seconds) is compatible with time scales of cognitive tasks.

Moreover, this makes it possible to observe metastable chimera states outside the areas of their existence, and we can form such transients by a pattern of initial conditions providing a potentially more flexible control over network dynamics. We will continue to study this phenomenon.

In addition, we considered the evolution of the chimera states observed in the largest area *Ch*1 of the parameter space. We found that depending on the synaptic strength and the connectivity parameter, the network can change the structure of the chimera states. For instance, it can transform the chimera states from static to traveling chimeras and from stationary to breathing chimera states.

SUPPLEMENTARY MATERIAL

In the supplementary material, we include additional information about the activity of the studied network. In particular, we describe properties of the chimera states in chimera regions complementary to the one considered in the main results (Ch2 and Ch3). Also, we consider the influence of neuronal excitability on the chimera states. For clarity, we further describe the regime of spiking death. In addition, we add technical information on how we have used the ACM approach for the study of evolution of the chimera states.

ACKNOWLEDGMENTS

The research leading to these results has received funding from the Basic Research Program at the National Research University

Higher School of Economics. This research was supported, in part, through computational resources of HPC facilities at HSE University. B.G. acknowledge support from the ANR Project ERMUNDY (Grant No. ANR-18-CE37-0014), CNRS, INSERM, ANR-17-EURE-0017, and ANR-10-IDEX-0001-02.

AUTHOR DECLARATIONS

Conflict of Interest

The authors have no conflicts to disclose.

Author Contributions

O. Dogonasheva: Conceptualization (equal); Formal analysis (equal); Investigation (equal); Methodology (equal); Software (equal); Visualization (equal); Writing – original draft (equal); Writing – review & editing (equal). **Dmitry Kasatkin:** Methodology (equal); Writing – review & editing (equal). **Boris Gutkin:** Funding acquisition (equal); Investigation (equal); Project administration (equal); Resources (equal); Supervision (equal); Writing – original draft (equal); Writing – review & editing (equal). **Denis Zakharov:** Conceptualization (equal); Investigation (equal); Methodology (equal); Project administration (equal); Supervision (equal); Validation (equal); Writing – original draft (equal); Writing – review & editing (equal).

DATA AVAILABILITY

The data that support the findings of this study are available from the corresponding author upon reasonable request.

REFERENCES

[1]D. Durstewitz and J. Seamans, "Beyond bistability: Biophysics and temporal dynamics of working memory," Neuroscience **139**, 119–133 (2006).
[2]A. Compte, "Computational and *in vitro* studies of persistent activity: Edging towards cellular and synaptic mechanisms of working memory," Neuroscience **139**, 135–151 (2006).
[3]N. Novikov, D. Zakharov, V. Moiseeva, and B. Gutkin, "Activity stabilization in a population model of working memory by sinusoidal and noisy inputs," Front. Neural Circuits **15**, 27 (2021).
[4]D. M. Abrams and S. H. Strogatz, "Chimera states for coupled oscillators," Phys. Rev. Lett. **93**, 174102 (2004).
[5]M. J. Panaggio and D. M. Abrams, "Chimera states: Coexistence of coherence and incoherence in networks of coupled oscillators," Nonlinearity **28**, R67 (2015).
[6]A. Destexhe, Z. F. Mainen, and T. J. Sejnowski, "Kinetic models of synaptic transmission," in *Methods in Neuronal Modeling*, 2nd ed. (MIT Press, 1998), pp. 1–25.
[7]A. Zakharova, M. Kapeller, and E. Schöll, "Chimera death: Symmetry breaking in dynamical networks," Phys. Rev. Lett. **112**, 154101 (2014).
[8]S. Song, P. J. Sjöström, M. Reigl, S. Nelson, and D. B. Chklovskii, "Highly nonrandom features of synaptic connectivity in local cortical circuits," PLoS Biol. **3**, e350 (2005).
[9]H. Sakaguchi, "Instability of synchronized motion in nonlocally coupled neural oscillators," Phys. Rev. E **73**, 031907 (2006).
[10]I. Omelchenko, E. Omel'chenko, P. Hövel, and E. Schöll, "When nonlocal coupling between oscillators becomes stronger: Patched synchrony or multichimera states," Phys. Rev. Lett. **110**, 224101 (2013).
[11]A. Calim, P. Hövel, M. Ozer, and M. Uzuntarla, "Chimera states in networks of type-I Morris-Lecar neurons," Phys. Rev. E **98**, 062217 (2018).
[12]B. K. Bera, D. Ghosh, and M. Lakshmanan, "Chimera states in bursting neurons," Phys. Rev. E **93**, 012205 (2016).
[13]Z. Wang, S. Baruni, F. Parastesh, S. Jafari, D. Ghosh, M. Perc, and I. Hussain, "Chimeras in an adaptive neuronal network with burst-timing-dependent plasticity," Neurocomputing **406**, 117–126 (2020).
[14]A. Mishra, S. Saha, D. Ghosh, G. V. Osipov, and S. K. Dana, "Traveling chimera pattern in a neuronal network under local gap junctional and nonlocal chemical synaptic interactions," Opera Med. Physiol. **3**, 14–18 (2017).
[15]T. Tateno, A. Harsch, and H. Robinson, "Threshold firing frequency–current relationships of neurons in rat somatosensory cortex: Type 1 and type 2 dynamics," J. Neurophysiol. **92**, 2283–2294 (2004).
[16]M. Tsodyks, "Attractor neural network models of spatial maps in hippocampus," Hippocampus **9**, 481–489 (1999).
[17]C. Morris and H. Lecar, "Voltage oscillations in the barnacle giant muscle fiber," Biophys. J. **35**, 193–213 (1981).
[18]O. Dogonasheva, D. Kasatkin, B. Gutkin, and D. Zakharov, "Robust universal approach to identify travelling chimeras and synchronized clusters in spiking networks," Chaos, Solitons Fractals **153**, 111541 (2021).
[19]D. Golomb, D. Hansel, and G. Mato, "Mechanisms of synchrony of neural activity in large networks," in *Handbook of Biological Physics* (Elsevier, 2001), Vol. 4, pp. 887–968.
[20]O. Dogonasheva, B. Gutkin, and D. Zakharov, "Calculation of travelling chimera speeds for dynamical systems with ring topologies," in *2021 5th Scientific School Dynamics of Complex Networks and Their Applications (DCNA)* (IEEE, 2021), pp. 61–64.
[21]E. L. Allgower and K. Georg, *Numerical Continuation Methods: An Introduction* (Springer Science & Business Media, 2012), Vol. 13.
[22]B. Bera, S. Rakshit, D. Ghosh, and J. Kurths, "Spike chimera states and firing regularities in neuronal hypernetworks," Chaos **29**, 053115 (2019).
[23]M. Rabinovich and P. Varona, "Robust transient dynamics and brain functions," Front. Comput. Neurosci. **5**, 24 (2011).